

# Dynamic Simulation of a Periodic 10 K Sorption Cryocooler

P. Bhandari, J. Rodriguez, S. Bard, and L. Wade

Jet Propulsion Laboratory  
California Institute of Technology  
4800 Oak Grove Drive  
Pasadena, CA USA 91109

## ABSTRACT

A transient thermal simulation model has been developed to simulate the dynamic performance of a multiple-stage 10 K sorption cryocooler for spacecraft sensor cooling applications that require periodic quick-cooldown (under 2 minutes), negligible vibration, low power consumption, and long-life (5 to 10 years). The model was specifically designed to represent the Brilliant Eyes Ten-Kelvin Sorption Cryocooler Experiment (BETSCE), but it can be adapted to represent other sorption cryocooler systems as well.

The model simulates the heat transfer, mass transfer and thermodynamic processes in the cryostat and the sorbent beds for the entire refrigeration cycle, and includes the transient effects of variable hydrogen supply pressure due to expansion and outflow of hydrogen during the cooldown operation. The paper describes model limitations and simplifying assumptions, with estimates of errors induced by them, and presents comparisons of performance predictions with ground experiments.

An important benefit of the model is its ability to predict performance sensitivities to variations of key design and operational parameters. The insights thus obtained are expected to lead to higher efficiencies and lower weights for future designs,

## INTRODUCTION AND BACKGROUND

A simulation model has been developed for the analysis and design of 10 K sorption cryocoolers. This paper describes the methodology used for developing and experimentally validating the model. Recommendations for improving the model fidelity and adapting it to other sorption cooler configurations are also presented.

Sorption cooler technology is ideal for many spacecraft sensor cooling applications because it provides negligible vibration, repeated quick cooldown capability, and low average power consumption. The continuous 10 K sorption cryocooler concept was originally conceived by Jones in 1984. <sup>1</sup>In 1991, Johnson and Jones developed the 10 K sorption periodic cryocooler concept and demonstrated that this cooler offers repeated quick cooldowns and low average power

consumption with intermittent operation.<sup>2</sup> The concept of a periodic 10 K hydrogen/ hydride sorption cryocooler was proven technically feasible in laboratory experiments carried out at JPL in 1991, which demonstrated the ability to cooldown in under 2 minutes and maintain an I<sup>2</sup>R simulated detector heat load of 150 mW below 10 K for over 30 minutes.<sup>3</sup> As a result of the success of these early experiments, a space qualified experimental cooler (BETSCE) was developed. BETSCE is mounted on the shuttle side wall, and was designed to be adaptable to the wide range of possible shuttle thermal environments, BETSCE qualification testing has been nearly completed.<sup>4</sup>

The basic periodic sorption cycle concept is based on alternately heating and cooling hydride powder beds to circulate hydrogen in a closed cycle and periodically cool a detector cold head assembly to 10 K on command. Fig. 1 shows the fluid schematic of the BETSCE instrument and a full detailed description can be found in Refs. 4-6. The BETSCE functional requirements are to:

- (1) Cooldown ins 2 minutes from > 60 K to a cold stage detector interface temperature of  $\leq 11$  K.
- (2) Sustain an I<sup>2</sup>R simulated detector heat load of > 100 mW at  $\leq 11$  K for  $\geq 10$  minutes.
- (3) Recycle the system in  $\leq 24$  hours.
- (4) Demonstrate  $\geq 3$  full repeatable cycles.
- (5) Record data required to characterize spaceflight/ microgravity performance of the 13 ETSCE instrument.

The cryostat subsystem model, including a description of the six cooldown phases and the thermodynamics of key system components, and the sorbent bed subsystem model are described in the following sections.

### DESCRIPTION OF TRANSIENT SIMULATION APPROACH

The BETSCE simulation model is constructed in two main modules: (1) the cryostat subsystem module which focuses on the thermodynamics of the blowdown process that produces first liquid and then solid H<sub>2</sub> from the pressurized gaseous H<sub>2</sub> stored in the supply tank, and (2) the sorbent

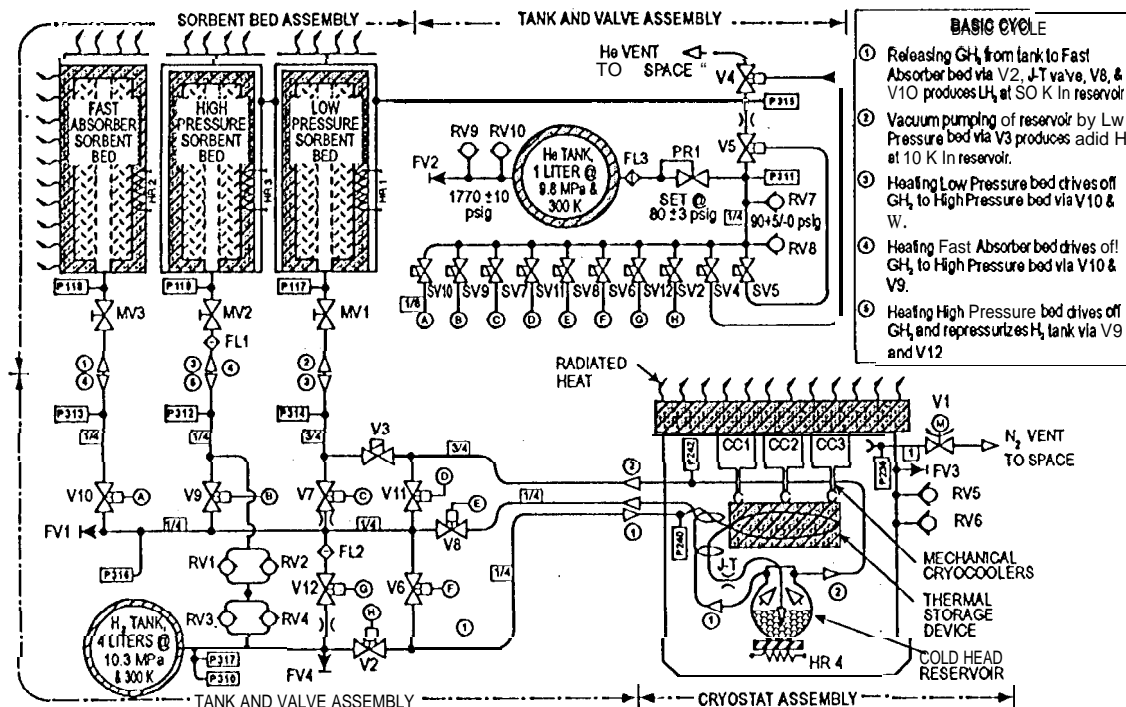


Figure 1. BETSCE fluid schematic.

bed subsystem model that focuses on recharging of the hydrogen supply tank after the 10 K cooling process is completed. The model modules were constructed using the lumped-capacitance approximation and were formulated into nodal networks for input to the Systems Improved Numerical Differencing Analyzer (SINDA) code. SINDA85 provided by NASA Goddard Space Flight Center and compiled under Microsoft Fortran power station was used to obtain solutions. This version of SINDA runs under Microsoft windows which provides great flexibility and ease of use when debugging, making changes, and analyzing the results.

Fortran subroutines were constructed to model the heat transfer and/or pressure drop in heat exchangers, plumbing lines, Joule-Thomson valve (J-T), cold head reservoir, radiators, hydride beds, and gas-gap heat switches. The thermodynamic and transport properties for gaseous and liquid normal hydrogen were obtained by linking the Cryodata GASPAC property prediction program to the SINDA85 model and making the appropriate subroutine calls. The solid H<sub>2</sub> properties obtained from NBS Monograph 168<sup>8</sup>, and other material properties were input to the model as temperature dependent arrays.

Cryostat Subsystem Model

**Cooldown Overview.** Fig. 2 illustrates the detailed fluid schematic “modeled. The blowdown process is initiated by opening valve V2 to release high pressure (~10 MPa) H<sub>2</sub> gas, which expands adiabatically through a J-T valve. The expansion lowers the H<sub>2</sub> gas temperature as it enters the cold head reservoir. This cold gas cools the reservoir and is exhausted to the fast absorber (FA) bed which maintains the low back pressure required for producing liquid H<sub>2</sub>. Before entering the J-T orifice, the H<sub>2</sub> gas is pre-cooled by a counter-flow heat exchanger (labeled WARM HX), a thermal storage device (TSD), and by another counterflow heat exchanger (labeled COLD HX). The COLD HX supply side gas stream is cooled by the counterflow cold gas stream exiting the cold head reservoir. Similarly, the WARM HX supply side gas stream is

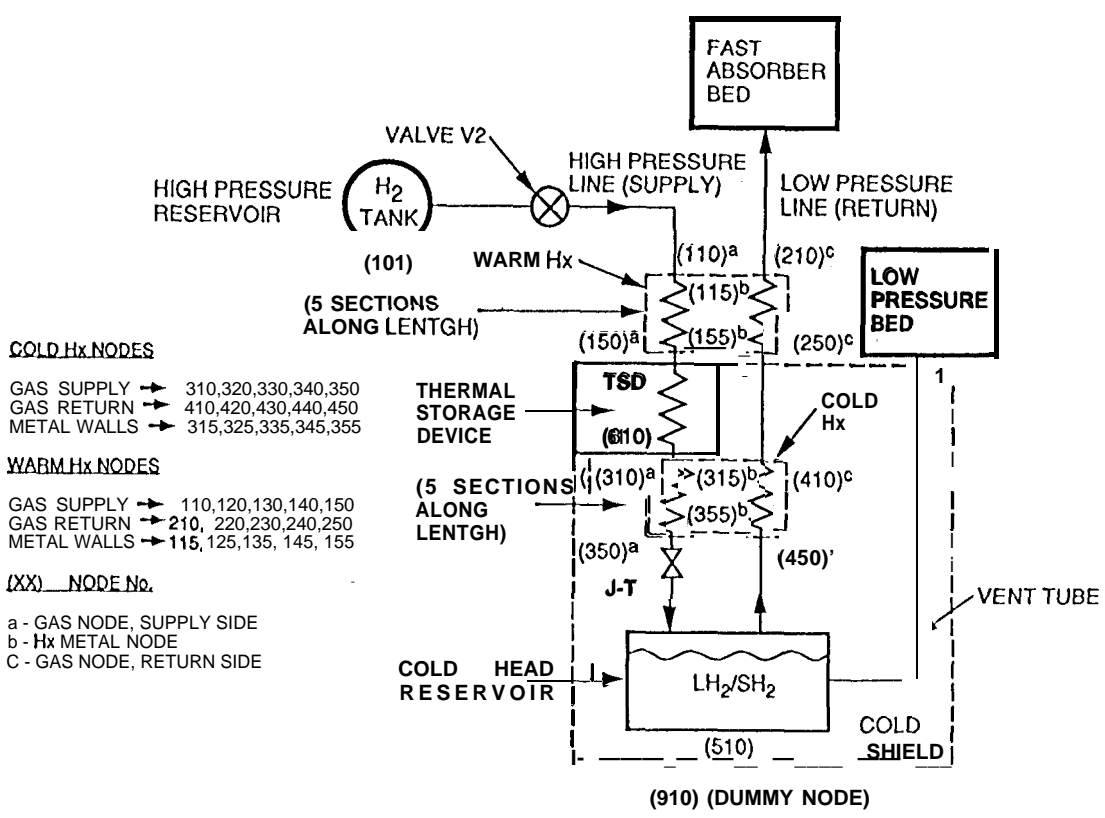


Figure 2. BETSCE detailed fluid schematic for simulation model.

cooled by the **counterflow** cold gas stream exiting the **COLD HX**. The **H<sub>2</sub>** gas exiting the supply side of the **WARM HX** is cooled by a single stream heat exchanger mounted to the **TSD**. Mechanical coolers maintain the **TSD** temperature at 60-70 K before each blowdown operation. The single-stream heat exchanger is designed for very high thermal effectiveness, and is thermally coupled to the **TSD** in a manner that results in minimal temperature gradients during the blowdown phase.

After the cold head cools below the **H<sub>2</sub>** dew point temperature, liquid **H<sub>2</sub>** produced at the **J-T** exit starts to accumulate in the wicked matrix within the cold head reservoir. Once an adequate amount of liquid **H<sub>2</sub>** is collected, the **H<sub>2</sub>** gas flow is stopped by closing **V2**. Then **V3** is opened, thus connecting the cold head to the low pressure (**LP**) bed. The **LP** bed is at a lower pressure than the saturation pressure of the liquid **H<sub>2</sub>** in the cold head, and thus serves as a vacuum pump that vaporizes the liquid **H<sub>2</sub>**. This vaporization process removes heat from the cold head and results in further cooling of the liquid **H<sub>2</sub>** until it freezes. Further pumping on the cold head cools the solid **H<sub>2</sub>** to below 10 K at which time the **1<sup>3</sup>R** simulated detector heat load is turned on. The simulated detector heat load provided by an electrical heater, plus the parasitic heat leak sublimate the solid **H<sub>2</sub>**, while the **LP** bed maintains a suitable back pressure ( $\leq 2 \times 10^{-4}$  MPa) to maintain the solid **H<sub>2</sub>** temperature at  $\leq 10$  K for  $\geq 10$  minutes. After all of the solid **H<sub>2</sub>** is sublimated, the system is ready for recycling.

**Cryostat Design Details.** The **TSD** is essentially an aluminum block (about 2,5 kg) with a thermal mass that is sufficient to limit its temperature rise to  $< 5$  K during the entire **blowdown** process ( $< 90$  seconds). A very high rate of energy transfer to the **TSD** occurs during this **quick-cooldown** process ( $\sim 1$  kW). The warm and cold heat exchangers are compact lightweight **counterflow** paired tube exchangers with a single central supply side tube surrounded by six brazed return side tubes, as shown in Fig. 3. The small diameter tubes (0.53 mm and 1.07 mm ID for cold and warm HXs, respectively), result in high convective heat transfer coefficients and high exchanger effectiveness. With the typical **BETSCE cryostat** mass flow rates of about 0.1 g/s during the blowdown process, these exchangers achieve high number of heat transfer units (**Ntu**), on the order of 10-15. During the blowdown process the pressure drops across these exchangers is  $\leq 0.3$  MPa, for both supply and return sides. Although the return side gas pressure is much lower than the supply side pressure, the flow cross-sectional area is six times larger (due to use of six tubes), which reduces the return side pressure drops to a suitable limit of  $\leq 0.3$  MPa.

The **FA** bed is specifically designed for the initial **cooldown** and liquid accumulation phase, and the **LP** bed is designed for producing solid **H<sub>2</sub>** and cooling down to  $\leq 10$  K. The **FA** bed hydride powder is thermally coupled via fins to a **Phase Change Material (PCM)**, which allows it to maintain temperature levels resulting in a dynamic hydride saturation pressure that is significantly lower than the critical pressure of hydrogen (33.2 K and 1.3 MPa). This allows production and accumulation of liquid **H<sub>2</sub>** during the blowdown process. Similarly, the thermal characteristics of the **LP** bed are designed such that it can maintain a temperature level that results in dynamic

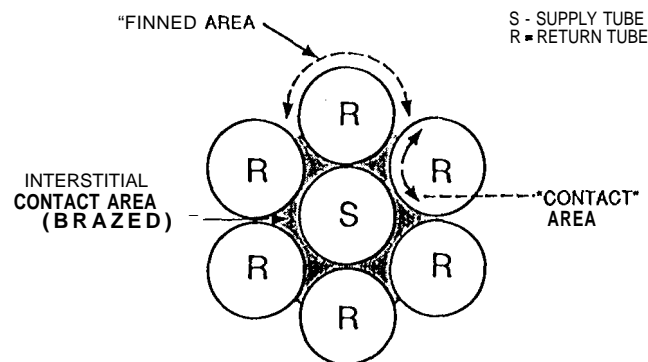


Figure 3. BETSCE paired tube heat exchanger construction,

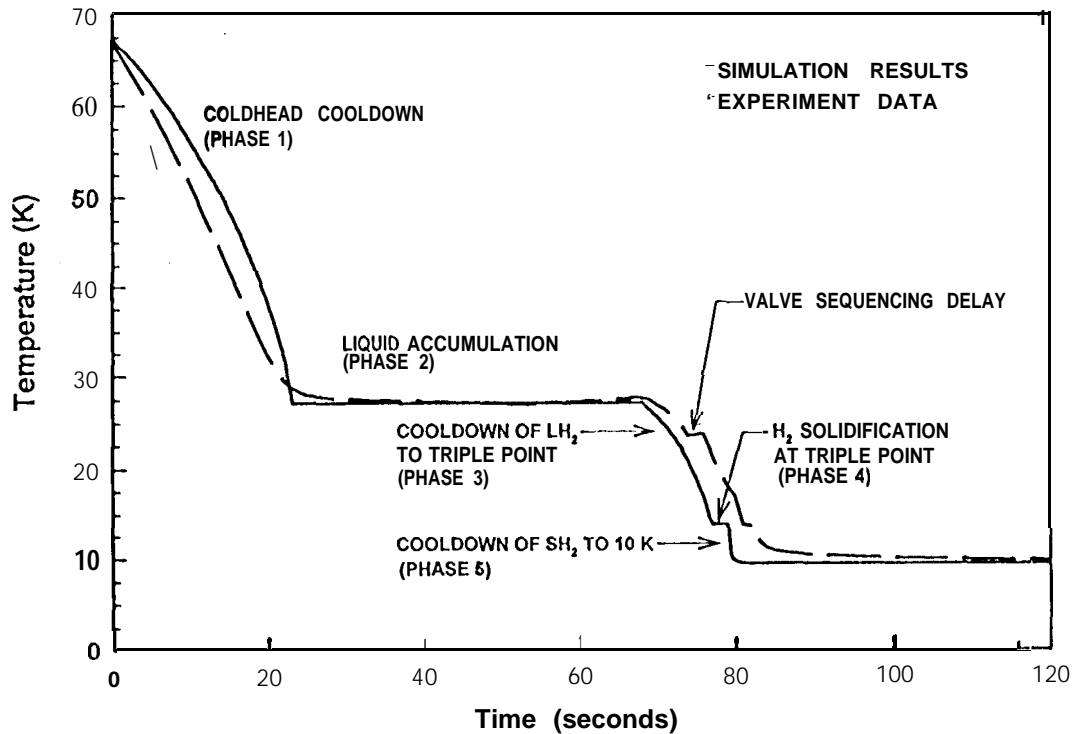


Figure 4, Comparison of theoretical prediction and experimental data for periodic 10 K BETSCE cooler; the separate cooling phases are indicated.

hydride saturation pressures below the hydrogen triple point pressure (13.95 K and 0.0072 MPa). This permits the production of solid hydrogen and the ability to cool to 10 K.

The vent tube is sized for low pressure drop while allowing the high mass flow rate ( $-0.02$  g/sec) of vaporized and sublimated gas required to produce solid  $H_2$  in under 30 seconds. Minimal pressure drop leads to minimal cold head temperature, but larger tube sizes lead to higher parasitic heat leaks. A trade-off analysis considering these competing effects was conducted to select suitable vent tube sizes for the three different temperature zones in the cryostat. The tube sizes are 0.81 cm, 1.13 cm, and 1.69 cm ID at the cold ( $< 60$  K), intermediate (60-150 K), and warm (150-300 K) temperature zones, respectively,

#### Phases of a Complete Cooldown Operation

The cold head cooldown from  $> 60$  K to  $< 32$  K, liquid accumulation at  $< 32$  K, cold head cooldown to  $\leq 10$  K, and the sublimation of solid  $H_2$  is separated into six distinct phases which are used as the basis for this model, as shown on Fig. 4. Table 1 presents the conservation equations for mass and energy in each phase.

**Phase 1: Cooldown of Cold Head Before Liquid Accumulation.** The cold head is cooled from  $\geq 60$  K to below 30 K through the bootstrap process shown in Fig. 5. The  $H_2$  gas, cooled by the J-T expansion, begins to cool the cold head reservoir. The heated gas exiting the reservoir pre-cools the high pressure supply side HX gas before the J-T inlet, and is finally absorbed by the FA bed. Any liquid produced in the J-T valve during this phase is immediately vaporized by heat from the warmer cold head. This phase continues until the cold head cools to a temperature equal to the  $H_2$  temperature exiting the J-T valve.

Table 1. Conservation equations for each cooldown phase.

Nomenclature:	
$t$ = time	$(MCp)_{ch}$ = thermal mass of cold head
$T_{ch}$ = temperature of cold head	$\dot{Q}_{par}$ = parasitic heat leak into cold head
$\dot{m}_v$ = mass flow rate of vapor leaving cold head	$h_l, h_v, h_s$ = enthalpy of saturated liquid, vapor and solid $H_2$ in cold head respectively
Cooldown Phase	Conserved Quantity
1. <u>Cooldown of cold head before liquid accumulation.</u>  $h_i$ = enthalpy of gas entering J-T $h_o$ = enthalpy of gas leaving cold head	mass: $\dot{m}_i = \dot{m}_o$ energy: $\dot{m}_i h_i - \dot{m}_o h_o = (MCp)_{ch} \frac{dT_{ch}}{dt}$
2. <u>Liquid accumulation.</u>  $h_g$ = enthalpy of saturated gas entering J-T $\dot{m}_g$ = mass flow rate of gas entering J-T $\dot{m}_l$ = liquid accumulation rate $\dot{m}_v$ = mass flow rate of saturated vapor leaving cold head	mass: $\dot{m}_g = \dot{m}_l + \dot{m}_v$ energy: $\dot{m}_g h_l = \dot{m}_v h_v + \dot{m}_l h_l$
3. <u>Cooldown of liquid to triple point.</u>  $M_l$ = instantaneous mass of liquid $H_2$ in cold head $M_{l,o}$ = mass of liquid $H_2$ at end of liquid accumulation phase $Cp_l$ = specific heat of liquid $H_2$ $\lambda_{l,v}$ = latent heat of vaporization of liquid $H_2$ ( $T_{ch}$ is assumed to equal the liquid $H_2$ temperature)	mass: $M_l = M_{l,o} - \int_0^t \dot{m}_o dt$ energy: $(M_l Cp_l + (MCp)_{ch}) \frac{dT_{ch}}{dt} = -\dot{m}_o \lambda_{l,v}$
4. <u>Solidification at triple point.</u>  $M_l$ = mass of liquid $H_2$ at beginning of this phase $M_s, M_v$ = mass of vapor and solid $H_2$ at end of this phase, respectively	mass: $M_l = M_s + M_v$ energy: $M_l h_l = M_s h_s + M_v h_v$
5. <u>Cooldown of solid <math>H_2</math> from triple point to 10 K.</u>  $M_s$ = instantaneous mass of solid $H_2$ in cold head $M_{s,o}$ = mass of solid $H_2$ at end of phase 4 $Cp_s$ = specific heat of solid $H_2$ $\lambda_{s,v}$ = latent heat of sublimation of solid $H_2$ ( $T_{ch}$ is assumed to equal the solid $H_2$ temperature)	mass: $M_s = M_{s,o} - \int_0^t \dot{m}_o dt$ energy: $(M_s Cp_s + (MCp)_{ch}) \frac{dT_{ch}}{dt} = -\dot{m}_o \lambda_{s,v} + \dot{Q}_{par}$
6. <u>Sublimation of solid <math>H_2</math> at 10 K.</u>  $M_{s,i}$ = mass of solid $H_2$ at end of phase 5 $\dot{Q}_{det}$ = simulated 1 <sup>2</sup> R detector heat load  (other variables have same meaning as in phase 5)	mass: $M_s = M_{s,i} - \int_0^t \dot{m}_o dt$ energy: $(M_s Cp_s + (MCp)_{ch}) \frac{dT_{ch}}{dt} = -\dot{m}_o \lambda_{s,v} + \dot{Q}_{par} + \dot{Q}_{det}$

Once this occurs, additional liquid produced is retained in the cold head reservoir wick. Note that the mass flow rates of gas entering and leaving the cold head are equal before the liquid accumulation phase begins.

**Phase 2: Liquid Accumulation.** During this phase, gas continues to flow through the J-T refrigeration loop and the liquid produced by the J-T expansion collects in the cold head for a

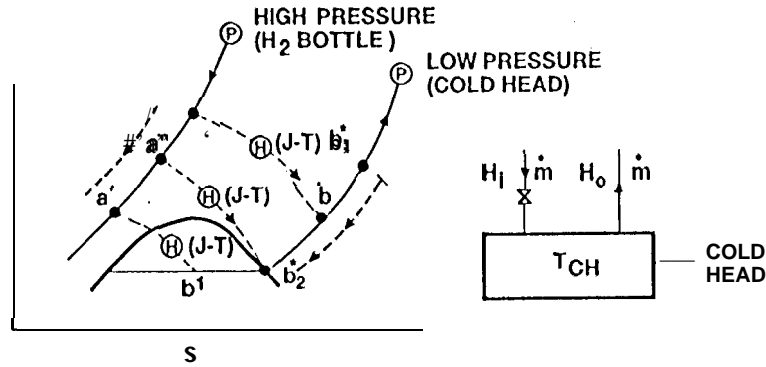


Figure 5. Bootstrap cooling of cold head reservoir before the liquid accumulation phase.

preset time period. The liquid yield during this phase is only about 15- 20%. The cold head temperature remains fairly constant with a slight decrease due to a small reduction in the J-T flow rate. This flow rate reduction leads to a lower return gas pressure, and therefore a lower saturation temperature in the cold head. Both the vapor exiting and remaining in the cold head are saturated (see Fig. 6). Combining the mass and energy conservation equations from Table 1 yields the liquid accumulation rate as:

$$m_1 = \dot{m}_g \frac{(h_v - h_g)}{\lambda} \quad (1)$$

where,

$\lambda$  = latent heat of vaporization

**Phase 3: Cooldown of Liquid to Triple Point.** When the liquid accumulation is over, valve V2 is closed to stop the J-T flow and the LP bed is activated by opening V7 followed by V3. The  $H_2$  saturation pressure of the ZrNi hydride in the LP bed is lower than that of the liquid in the cold head, which causes vapor to flow from the cold head to the LP bed via the high flow conductance vent line. The evaporation of liquid  $H_2$  removes heat from the remaining liquid  $H_2$  and cold head, resulting in a temperature decrease. This phase ends when the liquid  $H_2$  temperature reaches the triple point (13.95 K) (see Fig. 7a).

**Phase 4: Solidification at Triple Point.** When the cold head reaches the triple-point temperature, further vaporization solidifies the remaining liquid  $H_2$ , while the cold head

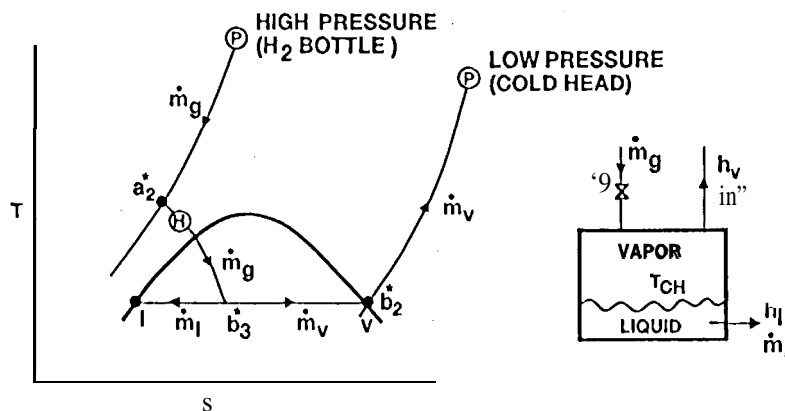


Figure 6. Liquid accumulation corresponding to phase 2.

temperature remains essentially constant (see Fig. 7b). Combining the mass and energy conservation equations from Table 1 yields a solution for the amount of solid  $H_2$  at the end this phase,

$$M_s = M_l \frac{\lambda_{l,v}}{\lambda_{s,v}} \quad (2)$$

where,

$\lambda_{l,v}$  = latent heat of vaporization

$\lambda_{s,v}$  = latent heat of sublimation

The time required to convert all of the liquid to solid  $H_2$  is determined from the following equation:

$$\Delta t = \frac{M_l}{\dot{m}_o} \left( 1 - \frac{\lambda_{l,v}}{\lambda_{s,v}} \right) \quad (3)$$

**Phase 5: Cooldown of Solid  $H_2$  from Triple Point to 10 K.** Once all the  $H_2$  is solidified, further pumping on the cold head by the LP bed removes latent heat of sublimation from the solid  $H_2$ . This further reduces the temperature of the solid  $H_2$  and cold head to  $\leq 10$  K, thus ending this phase, see Fig. 7c.

**Phase 6: Sublimation of Solid  $H_2$  at 10K.** The solid  $H_2$  at the end of phase 5 is now available to provide cooling to the simulated detector at a temperature level  $\leq 10$  K. The amount of hydrogen remaining at the beginning of this phase and the heat load on the cold head (including  $I^2R$  simulated detector heat load plus parasitic heat leaks) will determine the maximum detector cooling time available until all of the solid  $H_2$  is sublimated. The cold head temperature stabilizes after a short time when the total cold head heat load rate equals the heat removal rate from the sublimating solid  $H_2$ . When all of the solid  $H_2$  is consumed this phase ends and the hydride beds recycling operation begins.

### Thermodynamics of Key System Components

**Hydrogen Supply Tank** The pressure in the  $H_2$  supply tank is reduced as gas flows out during phases 1 and 2. The instantaneous pressure drop is dependent upon the resulting bulk temperature of the gas. The minimum reduction in pressure results for an isothermal expansion process. This occurs when there is good thermal coupling between the tank walls and the bulk gas, and the tank thermal mass is much larger than the gas thermal mass. The maximum reduction in pressure results for an adiabatic expansion process, if the thermal coupling between the bulk gas and the tank walls is poor, the gas expansion process is essentially adiabatic, and the gas temperature drops. This scenario is possible for large (especially spherical) supply tanks with central zones which have weak thermal coupling to the walls due to poor gas thermal conduction. BETSCE utilizes a single 4 liter cylindrical supply tank which provides a nearly isothermal

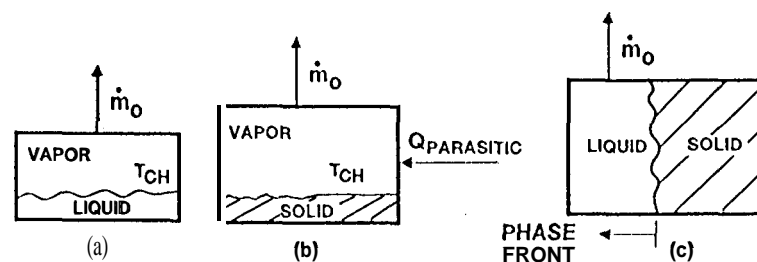


**Figure 7.** Cooldown of cold head to  $\leq 10$  K; (a) cooldown of liquid to triple point (phase 3), (b) solidification at triple point (phase 4), and (c) cooldown of solid  $H_2$  from triple point to  $\leq 10$  K (phase 5).

expansion as verified by experimental data. BETSCE is modeled with an isothermal supply tank; however, the program includes the option for modeling an adiabatic expansion process.

For an *isothermal* expansion the pressure drop is calculated from:<sup>9</sup>

$$\frac{P_2}{P_1} = \frac{m_2}{m_1}, \quad m_1 - m_2 = \int_1^2 \dot{m} dt \quad (4)$$

where,

- P = absolute pressure of gas in supply tank
- m = mass of gas in supply tank
- $\dot{m}$  = instantaneous mass flow rate of gas exiting supply tank
- 1,2 = refers to initial and final thermodynamic states

For an *adiabatic* expansion the pressure drop is as follows:<sup>9</sup>

$$\frac{P_2}{P_1} = \frac{m_2}{m_1} \left( \frac{T_2}{T_1} \right), \quad \frac{T_2}{T_1} = \left( \frac{m_2}{m_1} \right)^{k-1}, \quad m_1 - m_2 = \int_1^2 \dot{m} dt \quad (5)$$

where,

- k = 1.4, specific heat ratio for hydrogen =  $c_p/c_v$
- T = absolute temperature of gas in supply tank

Joule-Thomson Valve. The typical pressure range upstream of the J-T valve is from 6-10 MPa, whereas the downstream pressure is typically less than 0.6 MPa. Thus, the pressure ratio across the J-T valve is always less than the 0.53 limit required for choked flow through an orifice. Hence the choked flow mass flow rate can be calculated from:<sup>9</sup>

$$\dot{m} = A \cdot \frac{P_o}{\sqrt{T_o}} \sqrt{\frac{k}{R} \left( \frac{2}{k+1} \right)^{\frac{k+1}{2(k-1)}}} \quad (6)$$

where,

- A = flow cross-sectional area, m<sup>2</sup>
- k = 1.4, specific heat ratio for hydrogen
- R = 4124 m<sup>2</sup>/s<sup>2</sup>-K (gas constant for H<sub>2</sub>)
- P<sub>o</sub>, T<sub>o</sub> = stagnation pressure (Pa) and temperature (K), respectively

**Counterflow Heat Exchangers.** The warm and cold heat exchanger configuration is illustrated in Fig. 3. Each of these exchangers is divided into 5 equal axial sections in the model. The energy balance in a typical section is as follows (see Fig. 8):

$$(hA)_h (T_{h,o} - T_w) + (hA)_c (T_w - T_{c,o}) = (MCp)_w \frac{dT_w}{dt} \quad (7)$$

$$(\dot{m}c_p)_h (T_{h,i} - T_{h,o}) - (T_{h,o} - T_w)(hA)_h \quad (8)$$

$$(\dot{m}c_p)_c (T_{c,o} - T_{c,i}) - (T_w - T_{c,o})(hA)_c \quad (9)$$

where,

- h = convective heat transfer coefficient
- A = heat transfer area
- h,c = hot (supply side), cold (return side)
- w = wall
- (MCp)<sub>w</sub> = thermal mass of metal tube walls for each section
- m = mass flow rate
- c<sub>p</sub> = fluid specific heat
- i,o = in, out

The heat transfer and pressure drop in the exchangers were calculated using the following equations:

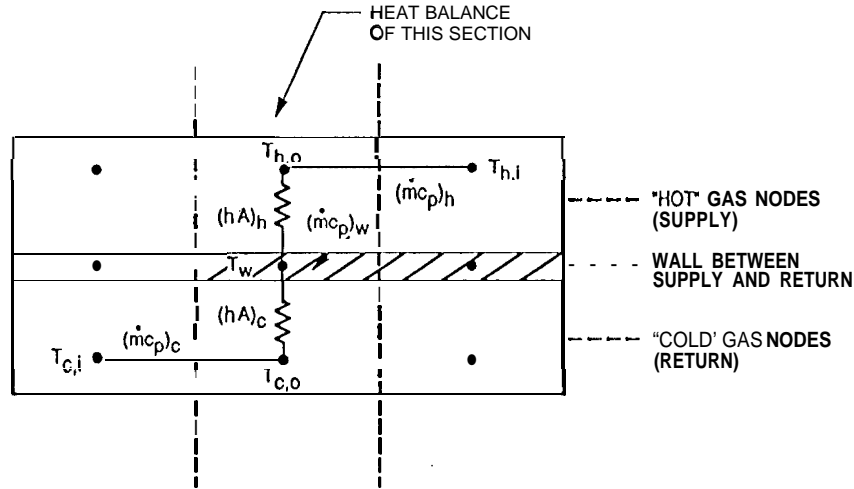


Figure 8. Heat exchanger thermal nodal network model.

laminar flow conditions ( $Re_d < 2300$ )<sup>10</sup>,

$$Nu = 4.364 \quad , \quad f = 64 / Re_d \quad (10)$$

turbulent flow conditions ( $Re_d > 2300$ )<sup>10</sup>,

$$Nu = 0.023 Re_d^{0.8} Pr^{0.33} \quad , \quad f = 0.316 Re_d^{-0.25} \quad (11)$$

where  $Nu$  and  $f$  are the Nusselt number and friction factor, respectively. The dimensionless Nusselt number is defined as:<sup>11</sup>

$$Nu = \frac{h d}{k} \quad (12)$$

where,

- $h$  = convective heat transfer coefficient
- $d$  = tube diameter
- $k$  = fluid thermal conductivity

For internal flows, the dimensionless friction factor is as follows:<sup>11</sup>

$$f = \frac{\Delta P}{\left(\frac{L}{d}\right) \frac{1}{2} \rho V^2} \quad (13)$$

where,

- $\Delta P$  = pressure drop
- $L, d$  = tube length and diameter, respectively
- $v$  = fluid velocity
- $\rho$  = fluid density

The dimensionless Reynolds number ( $Re_d$ ) for a tube is defined as:<sup>11</sup>

$$Re_d = \frac{Vd}{\nu} \quad (14)$$

where,

- $V$  = fluid velocity
- $d$  = tube diameter
- $\nu$  = fluid kinematic viscosity

The Prandtl number ( $Pr$ ) is a fluid property and is defined as the ratio of kinematic viscosity to thermal diffusivity.

The overall heat transfer conductance times the heat transfer area from supply and return side is calculated from:<sup>12</sup>

$$\frac{1}{(UA)_s} = \frac{1}{(UA)_r} + \frac{1}{(\eta_o hA)_s} + \frac{1}{(\eta_o hA)_r} + \frac{\delta}{(kA)_w} \quad (15)$$

where,

U = overall heat transfer conductance

$\eta_o$  = temperature effectiveness of total heat transfer area A

h = heat transfer coefficient

A = heat transfer area

s, r = supply, return

w = wall

$\delta$  = average wall thickness

k = thermal conductivity of metal wall

The temperature effectiveness of the total heat transfer area is given by the following equation:<sup>12</sup>

$$\eta_o = 1 - \frac{A_f}{A} (1 - \eta_f) \quad (16)$$

where,

$A_f$  = heat transfer area of fin

A = total heat transfer area

$\eta_f$  = fin efficiency

The exchanger *Ntu* is calculated from:<sup>12</sup>

$$Ntu = \frac{1}{(\dot{m} c_p)_{\min}} \int_0^A U dA \quad (17)$$

where,

$(\dot{m} c_p)_{\min}$  = minimum flow thermal capacity

From the geometry of the paired tube heat exchanger shown in Fig. 3, it is apparent that the six return side tubes will not have isothermal walls at any cross-section of the exchanger because only about 1/3 of the circumference is in contact with the inner supply tube. Consequently, it is necessary to approximate the return side tubes as having fins which permit the transfer of heat from the gas to the walls by convection, and then towards the "base" of the fin by circumferential conduction through the tube wall. The temperature effectiveness ( $\eta_o$ ) of the supply side tube is unity by definition. The fin efficiency ( $\eta_f$ ) for both warm and cold heat exchangers on the return side were calculated for a range of typical operating conditions. The cold heat exchanger has the highest **fin efficiency** with typical values ranging from 0.9 to 0.97. The warm exchanger has a broader fin efficiency range from 0.7 to 0.9. To simplify the **SINDA** model, constant **fin efficiencies** were used, with conservative values of 0.7 and 0.9 for the warm and cold heat exchangers, respectively. Accounting for the fin efficiency on the return side, the following temperature effectiveness for the exchangers was used:

$$\eta_o = \frac{1}{3} + \left\{ \frac{2}{3} \right\} \eta_f \quad (18)$$

**Computer Model of Complete Blowdown Operation,** A schematic of the simulation model and the nodal network is shown in Fig. 2. The heat exchangers are divided into 5 equal sections along their length. At each section there are 3 nodes, representing the supply side, return side and the tube walls. Hence, each exchanger is simulated by a total of 15 nodes. The **TSD** is modeled as a single node. The single-stream heat exchanger on the **TSD** has sufficient area to be treated as a perfect heat exchanger for all conditions, as verified by experimental data. The cold head is treated similarly because of the relatively large surface area of the wick matrix through which the hydrogen passes as it exits the reservoir.

The back Pressures in the FA and LP beds are assumed constant throughout the cooling phases. The hydride materials used are  $\text{LaNi}_{4.8}\text{Sn}_{0.2}$  and  $\text{ZrNi}$  for the FA and LP bed respectively. The hydride saturation pressures are computed using Vanat Hoff equation as follows:

$$\ln P_{\text{sat}} = b - a/T \quad (19)$$

where,

- T = absolute temperature of hydride material
- $P_{\text{sat}}$  = saturation plateau pressure of hydrogen in bed
- a,b = constants for each hydride material

The coefficients for the Van't Hoff equation are given in the following table: <sup>13</sup>

**Table 2. Van't Hoff coefficients for  $\text{ZrNi}$  and  $\text{LaNi}_{4.8}\text{Sn}_{0.2}$  hydride materials.**

Van't Hoff Equation Coefficients				
Hydride Material	Absorption Desorption	a (K)	b	Pressure Units
LP Bed $\text{ZrNi}$	Absorption	8018,738	21,311	torr
	Desorption	8251,06	14,492	atm
FA and HP Bed $\text{LaNi}_{4.8}\text{Sn}_{0.2}$	Absorption	4063.73	13.1515	atm
	Desorption	4024.34	12.5916	atm

**Numerical Solution Procedure.** The basic scheme used for integration of the differential equations in the time domain was to use small integration time steps ( $\leq 0.1$  see) while keeping the flow rates, pressures and masses of gaseous liquid or solid  $\text{H}_2$  constant within any time step, This permits SINDA to integrate the differential equations in time providing new temperature values for the next time step. A numerical sensitivity study was carried out to determine a suitable integration time step. Time steps ranging by two orders of magnitude were used to obtain solutions and the results indicated that, for time steps 0.1 seconds, the solutions were acceptably close. Similarly, a separate study was performed to determine the accuracy sensitivity to number of heat exchanger nodes. Again, the results showed that 5 sections provided reasonable accuracy when compared to the results for 10 or 15 sections,

### Sorbent Bed subsystem Model

**Overview of Recycle Operation.** After completing the last phase of the 10 K cooling operation, the next step is to commence the recycling operation and recharge the  $\text{H}_2$  tank. This is accomplished by heating the beds to suitable temperature levels to desorb the  $\text{H}_2$  at the required pressures, The LP and FA beds are first heated and pressurized to intermediate pressure levels to transfer the gaseous  $\text{H}_2$  to the high pressure (HP) bed. Then the HP bed is heated to desorb and pressurize the  $\text{H}_2$  to a high pressure of about 10 MPa. After completing the recharging process, all the beds are allowed to cool to their initial temperature before a new cold head cooldown is initiated,

**Hydride Sorption Fundamentals and Hardware Description.** During the 10 K cooldown operation,  $\text{H}_2$  is absorbed in the FA hydride bed releasing heat (exothermic reaction), which in turn increases its temperature. The temperature rise leads to an increase in the saturation pressure, which also reduces the rate of  $\text{H}_2$  absorption due to a reduction in driving force, The driving force is the difference between the pressure of the gas outside the bed and the hydride saturation pressure. Optimal bed designs minimize the temperature rise during absorption by having both a large thermal mass and a suitable thermal coupling to an external heat sink. During resorption, the LP and HP beds need to be thermally decoupled from the external heat sink to minimize heater power, These conflicting requirements for the LP and HP bed are met with the use of gas-gap heat switches. By filling the gas-gap with a suitable gas with good heat transport properties, such as helium or hydrogen, a strong thermal coupling to the external heat sink is achieved. A poor thermal coupling is obtained, when needed, by simply venting the gas to space.

During phases 1 and 2 of the **cooldown** operation, the **FA** bed absorbs  $H_2$  at rates which result in heat generation in excess of **1kW** for  $< 80$  seconds. To minimize the hydride temperature rise a phase change material (**PCM**) reservoir intimately coupled to the bed is utilized. A strong thermal coupling between the bed and the PCM heat sink is achieved by using high conductivity extended surfaces within the PCM reservoir. To recycle the FA, the entire bed including the PCM is heated to a suitable temperature that will not cause irreversible damage to the PCM, using heaters mounted to the beds.

Fig. 9 illustrates the **sorbent bed assembly (SBA)** configuration for **BETSCE**. Each bed has its own radiator (heat sink) sized accordingly for the different power dissipation and temperature level requirements.

### **Phases for Recharging the $H_2$ Tank**

The hydrogen gas absorbed in the LP and FA beds during the 10 K **cooldown** process is **desorbed** and pressurized in stages to recharge the supply tank to about **10 MPa**. The HP bed provides the final high level pressurization whereas the LP and FA beds provide the intermediate pressure levels. **After** completing the resorption, **all** the beds are cooled to their initial temperatures before commencing the next 10 K **cooldown** cycle. The following seven phases constitute the complete recycling operation.

**Phase 1: Desorption of LP Bed,** The LP bed contains **ZrNi** hydride which has a saturation pressure of about **1 MPa** at a temperature of **570 K**. This is a suitable pressure for transferring the  $H_2$  to the HP bed, where it is absorbed. During this phase the LP bed heater is on at full power and the gas-gap switch is off (evacuated). An equivalent effective thermal capacitance for this resorption process is obtained by simply calculating the total heat of reaction required to drive off **all** the absorbed  $H_2$  and dividing this quantity by the bed temperature rise (initial temperature to **570 K**). In the simulation, this phase is modeled by increasing the hydride normal thermal capacitance by this equivalent thermal capacitance to account for the heat of reaction. In **BETSCE**, the LP bed desorbs about **1 g** of  $H_2$ , and the typical resorption temperature rise is about **300 K** (**270 K** to **570 K**), which results in an increase in the effective thermal capacitance by about **114 J/K**. The resorption heat of reaction for **ZrNi** is **34.2 kJ/g<sup>o</sup>**. In **BETSCE**, the LP bed heater has a peak power level of **180 W**.

**Phase 2: Resorption in LP Bed and Simultaneous Absorption in the HP Bed.** After the  $H_2$  is pressurized in the LP bed to  $\sim 1$  MPa, valves **V9** and **V7** are opened to allow gas to transfer to the HP bed, where it is absorbed. At this point the LP bed heater is cycled **on/off** to maintain a temperature of **570 K**. This process is continued for about **10 minutes** to allow for all the  $H_2$  to be absorbed in the HP bed. It is assumed that all of the  $H_2$  gas is **desorbed** in phase 1, and thus the thermal capacitance of the LP bed is not modified in this phase. However, the heat of absorption is added to the HP bed to properly account for the rate of heat generated. For **BETSCE** this amounts to an average of about **30 W**. The heat of reaction for **LaNi<sub>0.8</sub>Sn<sub>0.2</sub>** is **17.1 kJ/g<sup>o</sup>**. Ideally, the gas-gap heat switch in the LP bed should be off and in the HP bed it should be on. However, in **BETSCE** both gas-gap switches are connected in order to minimize the number of valves, and are **left off** during this phase. This is not a problem because the total heat of reaction generated in the HP bed is relatively small and the resulting hydride temperature rise is not very significant.

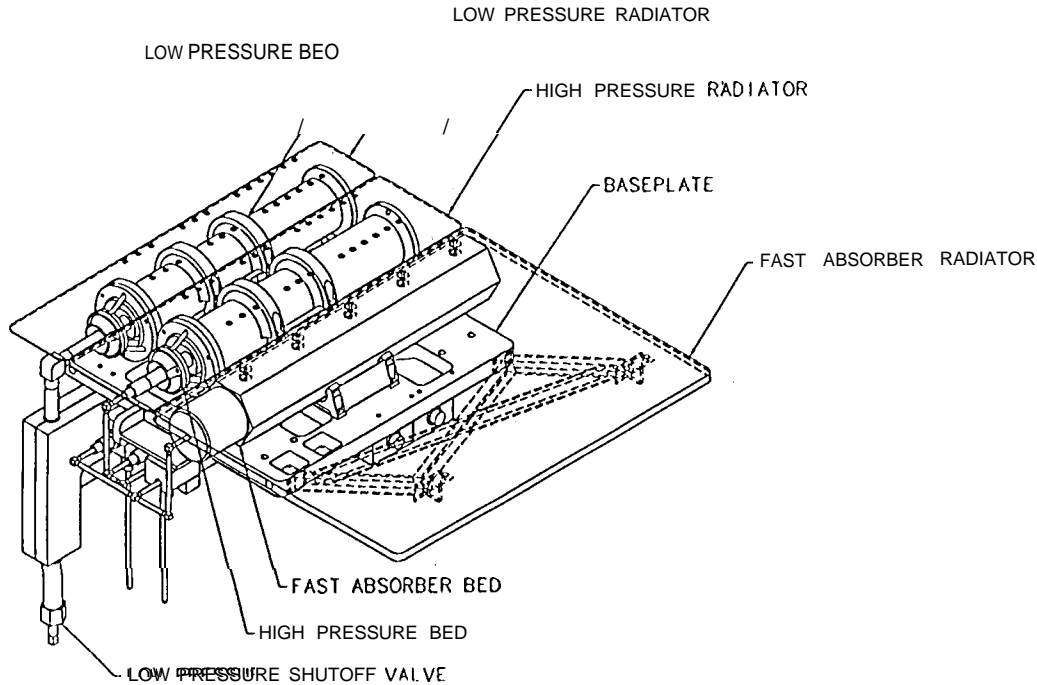


Figure 9. 13 ETSCE sorbent bed assembly configuration.

**Phase 3: Desorption of  $H_2$  in the FA Bed.** This phase is similar to the desorption of  $H_2$  from the LP bed except for the operating parameters. In this case, the FA bed is heated to 355 K, which results in a saturation pressure of about 3 MPa. The FA bed heater is on at full power (180 W for BETSCE). In BETSCE the FA bed absorbs about 6 g of  $H_2$  which results in an additional effective thermal capacitance of about 1280 J/K. Valves V10 and V9 which connect the FA to the 11P, are closed in this phase.

**Phase 4: Desorption in FA Bed and Simultaneous Absorption in 11P Bed.** Again this phase is similar to phase 2. However, the heater power is cycled for 20 minutes to maintain the bed temperature at 355 K. The gas-gap heat switch in the HP bed is turned onto minimize the hydride temperature rise. In BETSCE, the absorption of 6 g of  $H_2$  in the HP bed results in about 85 W for 20 minutes. This is about three times the power level generated in phase 2.

**Phase 5: Desorption in HP Bed.** This phase accomplishes the final pressurization required to transfer gas to the  $H_2$  tank. In this case, the HP bed is heated to 510 K which corresponds to a saturation pressure level of  $> 10$  MPa. In the model, the heat of resorption is again accounted for by increasing the thermal capacitance of the hydride by an equivalent thermal capacitance. In BETSCE the HP bed absorbs about 7 g which results in an increase in the effective thermal capacity by 498 J/K. BETSCE's HP bed heater maximum power is 180 W. Valves V9 and V12 connecting the HP bed to the tank are closed, and the gas-gap heat switch is off,

**Phase 6: Desorption in HP Bed and Simultaneous Filling of  $H_2$  Tank.** This phase is similar to phase 4, and it also takes 20 minutes to complete. The heater is cycled to maintain 510 K and the gas-gap heat switch remains off. Valves V9 and V12 are opened to fill the  $H_2$  tank.

**Phase 7: Cooldown of All Hydride Beds to Initial Temperatures.** This is the final phase of the recycling operation when all the hydride beds are allowed to cooldown until the PCM in the

FA bed refreezes. After the PCM is frozen, the FA bed is ready to absorb  $H_2$  in the next blowdown operation, In this phase the gas-gap heat switches are on to reject heat, via the radiators, from the sorbent beds to allow them to cool down as rapidly as possible. Once the PCM temperature drops below its freezing point temperature the entire system is ready commence the next blowdown operation.

### Computer Model of Hydride Beds for the Recycling Operation

Fig. 10 illustrates the nodal network used to model the SBA. Each hydride bed is modeled with a single node representing the hydride material and its tube, another node is used for the housing and a separate node is used for the radiator, The FA bed has an additional node for the PCM and its fins which are between the hydride tube and the housing. The gas-gap heat switches are modeled as conductors which can be turned on or off. Only the LP and HP beds have gas-gap heat switches. The model assumes the radiators are painted with white paint with an solar absorptivity ( $\alpha$ ) of 0.2 and an infrared emissivity ( $\epsilon$ ) of 0.85. The PCM freezing point temperature and latent heat of fusion were assumed to be  $17.5^\circ C$  and  $211.5 \text{ kJ/kg}$ , respectively (properties for n-Hexadecane used in BETSCE).<sup>13</sup> The only input required for the model is an average effective sink temperature for the radiators which is determine from the shuttle orbit and orientation. The nominal earth-viewing shuttle orientation results in an effective sink temperature of  $-12^\circ C$  for a surface with an  $\epsilon/\alpha$  ratio of 0,2/0.85.

### SIMULATION MODEL RESULTS AND COMPARISON WITH GROUND EXPERIMENT DATA

The BETSCE cryostat assembly was built by APD Cryogenics and the sorbent bed assembly was built by Aerojet, both subsystems were delivered to JPL in late 1993, The cryostat was integrated to the SBA and the tank and valve assembly (TVA) at JPL. System-level test results show that both the cryostat and the SBA meet their functional requirements.

**Cryostat Subsystem Simulation Results.** A typical blowdown scenario from the functional testing carried out at JPL was selected to make comparisons with the model results. Fig. 4 shows the comparison between model predictions and test data. At the start of a blowdown operation, the vent tube cross (see Fig. 11) temperature is close to the TSD temperature. During phases 1 and 2 of the blowdown, the vented  $H_2$  gas from the cold head enters the cold heat exchanger near the warmer vent tube cross, resulting in a parasitic heat leak into the cold heat exchanger. From the test data, this parasitic heat leak is about 2 W, and this fixed value was included in the model.

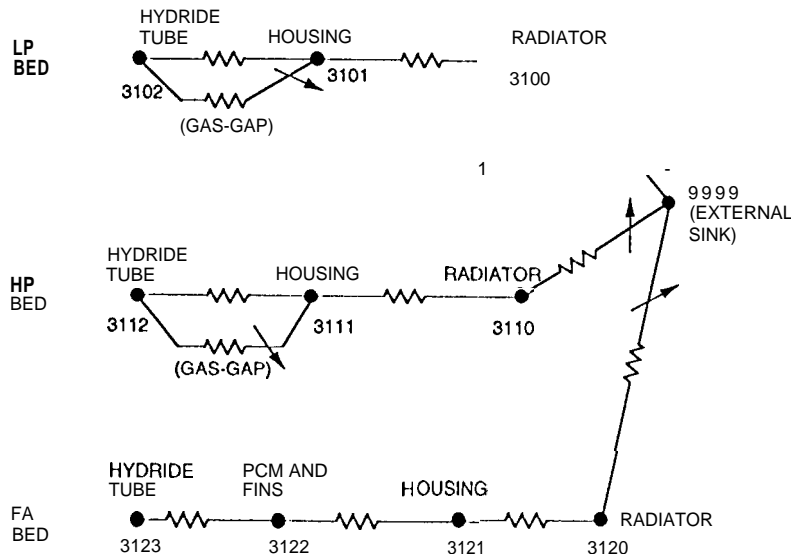


Figure 10. Sorbent bed assembly thermal nodal network model.

Comparison of results in Fig. 4 show an agreement of better than 51% in the predicted duration for phases 1 through 3. The model input parameters and key results are shown in Tables 3 and 4.

The major discrepancy between the simulation results and the test data is in the prediction of the time required for phase 5. This is primarily due to the high vent rate predicted by the model in this phase when the cold head temperatures and pressures are both very low. It is believed that this is due to severe compressible flow effects in the vent tube. The model does simulate this phenomena, but only to a limited simplified extent. Detailed modeling of compressible flow effects should minimize this discrepancy. In addition, the model underpredicts by about 15% the mass flow rate from the supply tank during phases 1 and 2. The predicted TSD temperature rise is also somewhat higher than test data. These latter two discrepancies need further investigation.

**Sorbent Bed Subsystem Simulation Results.** Solutions were obtained with computational time steps of 100 seconds and typical recycle times were about 13 hours for the nominal earth-viewing shuttle orbit. Fig. 12 shows the hydride bed temperatures as a function of time. Note that the time constant for cooling the beds is much higher than the shuttle orbit period (~1.5 hours), and thus using an average space sink temperature is a reasonable assumption. Results from planned ground tests will be used to calibrate the sorbent bed subsystem simulation model.

## MODEL BENEFITS TO 10 K SORPTION COOLER DESIGNS

Design tool to enable development of lightweight flight 10 K sorption cryocoolers.

Planned parametric studies will lead to an understanding of performance sensitivities to varying key parameters, such as heat loads, cooling duration, tank size and pressure, and thermal environment.

Enable microgravity effects to be quantified by comparing flight data, ground test data, and model results.

Model can be easily adapted to other configurations, such as a two-bed system that eliminates the FA bed, as well as to continuous cooler designs. Much of the modeling methodology is identical, or very similar to the BETSCE model described here.

## SUMMARY AND CONCLUSIONS

The simulation model developed for the BETSCE cryostat predicts the ground-based performance quite well, as verified by experimental data. It is anticipated that better fidelity will be obtained in the future when the following improvements are incorporated in the model:

- Improved detailed simulation of flow dynamics with choking in the high conductance vent tube. The low pressure (~1 torr) in the vent tube leads to high flow velocities and at room temperature high Mach numbers  $\leq 1$  are achieved.  
Improved simulation of actual valve sequencing between phases and the corresponding heat and mass transfer dynamics,
- More rigorous simulation of the actual heat transfer phenomena observed between the cold head and cold heat exchanger during phases 1 and 2 which leads to a parasitic heat leak on the cold heat exchanger. At the start of a blowdown operation, the vent tube cross temperature is near the TSD temperature. The cold vented H<sub>2</sub> gas from the cold head passes through the vent tube cross prior to entering the cold heat exchanger resulting in a parasitic heat leak.
- Integration of the cryostat model to sorbent bed subsystem model.

**Table 3. Input parameters for cryostat simulation.**

Input Parameters	Units	Model	Test Data
1. Initial conditions			
Cold head temperature	K		67.4
TSD temperature	K		60.6
Average cold / warm HX temperatures	K		84/117 <del>8</del>
Supply tank pressure	MPa		10.94
2. FA bed pressure	MPa		0.16
3. LP bed pressure	Torr		1
4. J-T effective orifice size	roils		4
5. Mass of vent tube added to cold head mass	g		18
6. Cold head parasitic heat load	mW		35
7. Cold heat exchanger parasitic heat leak (due to vent tube cross cooldown)	w		2.2
8. Liquid accumulation time	sec		45
9. Simulated I <sup>2</sup> R detector heat load	mW		100
10. Initial H <sub>2</sub> mass in supply tank	g		34.36

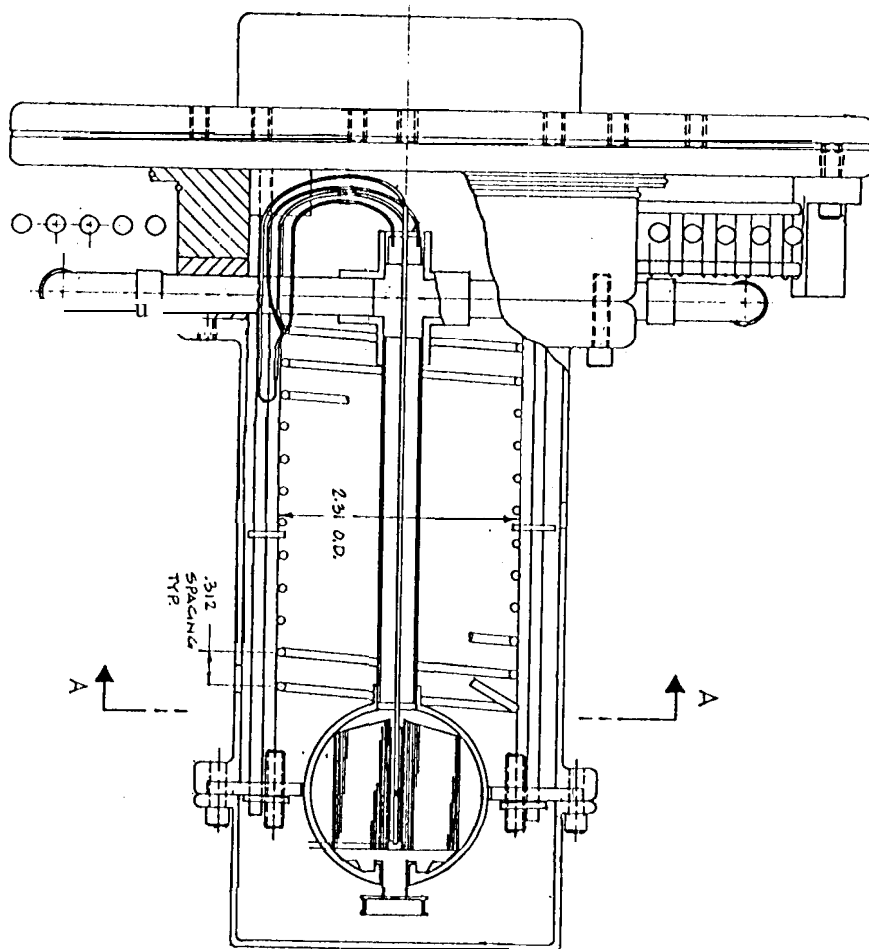


Figure 11, BETSCE thermal storage device subassembly.

*Input Parameter*

**Table 4.** Key results from cryostat simulation.

Parameters	Units	Model	Test Data
<b>10 K cooldown phases</b>			
<b>1. Initial cooldown before liquid accumulation</b>			
Time for this phase	s	23.3	24
J-T flow rate range	mg/s	115→130	
Conditions at end of phase			
J-T inlet temperature	K	42.3	
Tank pressure	MPa	10.09	
Cold head temperature	K	27.2	
Cold head pressure	MPa	0.51	
Refrigeration effect on cold head	W	15.1	
Warm / Cold HX Ntu		17.3/ 13.4	
TSD temperature	K	70.6	
AP high/ low pressure line	MPa	0.30/ 0.35	
<b>2. Liquid accumulation</b>			
Time for this phase (input parameter)	s	45	45
Liquid accumulated	g	0.83	
J-T flow rate range	mg/s	125	
Average liquid yield	%	16.8	
Conditions at end of phase			
J-T inlet temperature	K	47	
Tank pressure	MPa	8.46	
Cold head temperature	K	27.2	
Cold head pressure	MPa	0.51	
Warm / Cold HX Ntu		18.7/ 17.5	
TSD temperature	K	70.6→77.2	
Total H <sub>2</sub> gas consumption from supply tank (phase 1 & 2)	g	8.2	9.76
<b>3. Cooldown to triple point</b>			
Time for this phase	s	8.8	
Vent tube H <sub>2</sub> flow rate	mg/s	31.8	
Remaining liquid H <sub>2</sub> at end of phase	g	0.552	
<b>4. Solidification at triple point</b>			
Time for this phase	s	2	
Vent tube H <sub>2</sub> flow rate	mg/s	31.8	
Remaining solid H <sub>2</sub> at end of phase	g	0.488	
<b>5. Subcooling to 11K</b>			
Time for this phase	s	0.34	
Vent tube H <sub>2</sub> flow rate	mg/s	31.8	
Remaining solid H <sub>2</sub> at end of phase	g	0.478	
<b>6. Cooling of simulated detector</b>			
Steady state vent tube H <sub>2</sub> flow rate	mg/s	0.285	
Steady state cold head temperature	K	9.48	
<b>7. Entire blowdown process</b>			
Total time for phases 1 through 5	s	79.5	78

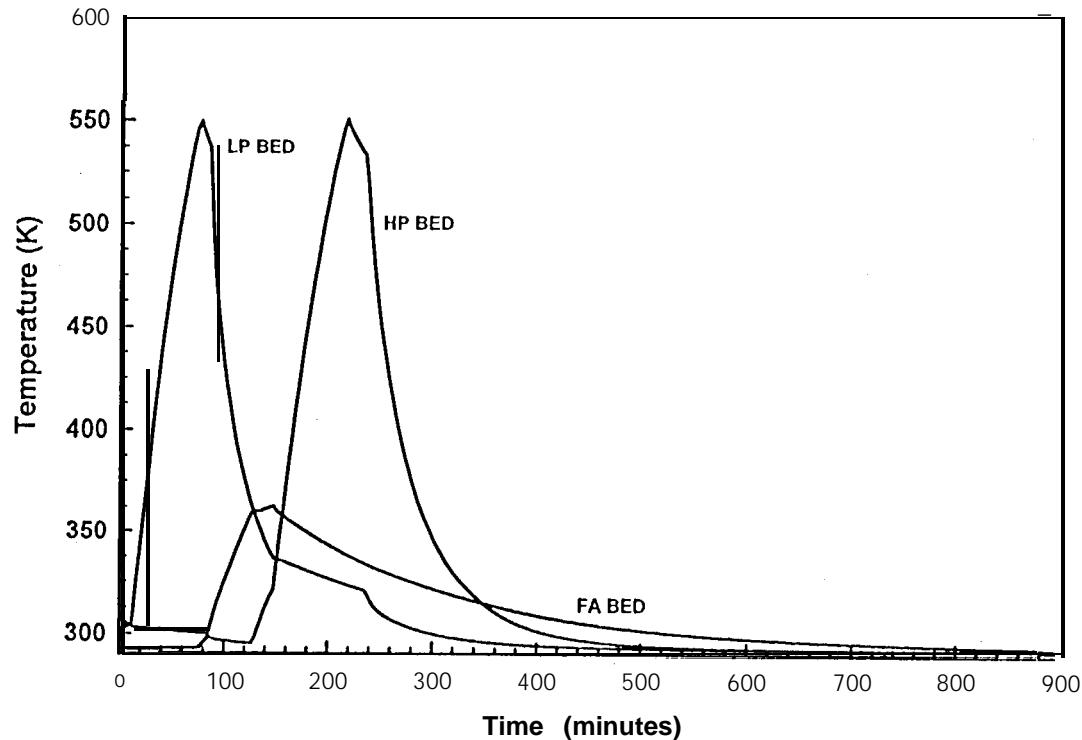


Figure 12. BETSCE SBA predicted performance for nominal earth-viewing shuttle orientation,

This model can be adapted to other sorption cooler configurations fairly easily because the basic model building blocks for the cooler components have been developed. Operating parameters can be easily changed to understand the performance sensitivities and carry out optimization trades. This simulation tool will aid in the design of future lightweight, **efficient**, sorption **cryocoolers** for surveillance, astrophysics astronomy, planetary and earth observation satellite cooling applications.

## ACKNOWLEDGMENTS

The work described in this paper was carried out by the Jet Propulsion Laboratory (JPL), California Institute of Technology under contract with the National Aeronautics and Space Administration. The work was sponsored by the Brilliant Eyes program office, Ballistic Missile and Defense Organization (BMDO), USAF Space and Missiles Systems Center (SMC). The contributions of Phil Sywulka of Aerojet in the initial development of the sorbent bed thermal nodal model are appreciated.

## REFERENCES

1. Jones, J. A., "Hydride Absorption Refrigerator System for Ten Kelvin and Below," Proceedings of the Third Cryocooler Conference, NBS Special Publication 698, NBS, Boulder, CO, (1984).
2. Johnson, A. L. and Jones, J. A., "Evolution of the 10 K Periodic Sorption Refrigerator Concept," Proceedings of the 7th International Cryocooler Conference, PL-CP-93-1001, Phillips Laboratory, Kirtland AFB, NM, (1993), pp. 831-853.
3. Wu, J. J., Bard, S., Boulter, W., Rodriguez, J., and Longworth, R., "Experimental Demonstration of a 10 K Sorption Cryocooler Stage," Advances in Cryogenic Engineering, Vol. 39, Plenum Press, New York, NY (1994), in press.

4. Bard, S., Wu, J., Karlmann, P., Cowgill, P., Mirate, C., and Rodriguez, J., "Ground Testing of a 10 K Sorption Cryocooler Flight Experiment (BETSCE)," Proceedings of the 8th International Cryocooler Conference, Vail Colorado, June 28-30, 1994.
5. Bard, S., Cowgill, P., Rodriguez, J., Wade, L., Wu, J. J., Gehrlein, M., Von Der Ohe, W., "10 K Sorption Cryocooler Flight Experiment (BETSCE)," Proceedings of the 7th International Cryocooler Conference, PL-Cp-93-100 1, Philips Laboratory, Kirtland AFB, NM, (1993), pp. 1107-1 119.
6. Bhandari, P. and Bard, S., "Thermal Systems Design and Analysis for a 10 K Sorption Cryocooler Flight Experiment," AIAA 28th Thermophysics Conference, AIAA 93-2825, Orlando, FL (1993).
7. McCarty, R.D., and Arp, V., "GASPAK v3," User's Guide to GASPAK Version 3.0, Copyright byCryodata(1990).
8. McCarty, R.D., Herd, J., and Roder, H, M., "Selected Properties of Hydrogen (Engineering Design Data)," NBS Nomograph168, U. S. Government Printing Office, Washington (1981),
9. Zucrow, M. J., and Hoffman, J.D., "Gas Dynamics," John Wiley& Sons, New York (1976), pp. 172-175.
10. Edwards, D. K., Denny, V.E., and Mills, A. F., "Transfer Processes," 2nd Ed., McGraw-Hill Book Company, New York (1979), pp. 166-167.
11. Mills, A.F., "Heat Transfer," 1st Ed., Irwin Book Company, Homewood, IL (1992).
12. Kays, W.M. and London, A.L., "Compact Heat Exchangers," 2nd E., McGraw-Hill Book Company, New York (1964), pp. 10-37.
13. Wade, L. A., Bowman, R. C., Gilkinson, D. R., and Sywulka, P. H., "Development of Sorbent Bed Assembly for a Periodic 10 K Solid Hydrogen Cryocooler," Advances in Cryogenic Engineering, Vol. 39, Plenum Press, New York, NY (1 994), in press.